Chinese Journal of Chemical Engineering 53 (2023) 46–55

Contents lists available at ScienceDirect

Chinese Journal of Chemical Engineering

journal homepage: www.elsevier.com/locate/CJChE

Full Length Article

Entropy generation analysis from the time-dependent quadratic combined convective flow with multiple diffusions and nonlinear thermal radiation

P.M. Patil [1,2,*], Bharath Goudar [1]

[1] Department of Mathematics, Karnatak University, Pavate Nagar, Dharwad 580003, India
[2] Wrangler Dr. D. C. Pavate Institute of Mathematical Sciences, Karnatak University, Dharwad 580003, India

ARTICLE INFO

Article history:
Received 6 December 2021
Received in revised form 15 January 2022
Accepted 18 January 2022
Available online 25 January 2022

Keywords:
Unsteady flow
Entropy
Radiation
Quasilinearization technique
Numerical analysis
Quadratic combined convection

ABSTRACT

Diffusions of multiple components have numerous applications such as underground water flow, pollutant movement, stratospheric warming, and food processing. Particularly, liquid hydrogen is used in the cooling process of the aeroplane. Further, liquid nitrogen can find applications in cooling equipment or electronic devices, *i.e.*, high temperature superconducting (HTS) cables. So, herein, we have analysed the entropy generation (EG), nonlinear thermal radiation and unsteady (time-dependent) nature of the flow on quadratic combined convective flow over a permeable slender cylinder with diffusions of liquid hydrogen and nitrogen. The governing equations for flow and heat transfer characteristics are expressed in terms of nonlinear coupled partial differential equations. The solutions of these equations are attempted numerically by employing the quasilinearization technique with the implicit finite difference approximation. It is found that EG is minimum for double diffusion (liquid hydrogen and heat diffusion) than triple diffusion (diffusion of liquid hydrogen, nitrogen and heat). The enhancing values of the radiation parameter R_d and temperature ratio θ_w augment the fluid temperature for steady and unsteady cases as well as the local Nusselt number. Because, the fluid absorbs the heat energy released due to radiation, and in turn releases the heat energy from the cylinder to the surrounding surface.

1. Introduction

In nature or industries, every flow problem is connected with time *i.e.*, the flow will be of unsteady (time-dependent) nature. For example, biological and geophysical flows, nuclear reactor cooling, materials processing, solar central receivers exposed to wind currents, stall flutter of helicopter blades, flow through turbomachinery blades, *etc.* Here the flow will depend on time. Due to the troublesome approach in solving unsteady flow problems [1–4], many researchers avoid it and concentrate only on steady flow problems. However, Noor *et al.* [1] have worked on unsteady combined convection flow near a porous three-dimensional body in a viscous fluid's stagnation point. Kumari and Nath [2] analysed time-dependent combined convective flow on a semi-infinite vertical plate. Ghalambazab *et al.* [3] have investigated the effect of nano-encapsulated phase change materials (NEPCMs) in a permeable medium with time variations. The impact of moving slender cylinder was considered by Roy and Anilkumar [4] in an unsteady combined convection regime.

Triple diffusion occurs when temperature and two species concentration diffusions coexist. Underground water flow, pollutant movement, acid rain effects, stratospheric warming, contaminant transport, food processing and many more are all examples where triple diffusive (multiple diffusion) mixed convection can be useful. In literature, there are limited studies made on the mixed convective triple diffusion flow. Khan *et al.* [5], Ghalambaz *et al.* [6], Khan *et al.* [7], confined their study only to natural convective triply diffusion flow. At the same time, Patil *et al.* [8–10] and Ghalambaz *et al.* [11] extended their work by taking combined convection flow with triple diffusion. Diffusion of liquid nitrogen and hydrogen are considered in this study as they have a lot of applications in heat and mass transfer processes. For instance, liquid hydrogen is used in the cooling process of the aerospace plane [12]. Liquid nitrogen can find applications in cooling equipment or electronic devices, *i.e.*, high temperature superconducting (HTS) cables [13]. Also, in food freezing and to

* Corresponding author at: Department of Mathematics, Karnatak University, Pavate Nagar, Dharwad 580003, India.
E-mail address: pmpatil@kud.ac.in (P.M. Patil).

https://doi.org/10.1016/j.cjche.2022.01.013
1004-9541/

cool soft or heat-sensitive materials at room temperatures like plastics, certain metals, tires, and pharmaceuticals [14]. Al-Garni *et al.* [12] concluded that liquid hydrogen outperforms liquid methane as a cooling medium.

Flows past a cylinder are normally regarded as two-dimensional if the body radius is greater than the thickness of the boundary layer. For a slender cylinder, the radius of the cylinder may be of the same order as that of the boundary layer thickness. Therefore, in the case of a slender cylinder, axisymmetric flow is taken into account rather than a two-dimensional flow. Two surface curvatures, the transverse in a plane normal to the axis of symmetry and the longitudinal in the meridian plane, characterise the flow along a thin cylinder [4]. The centrifugal force caused by the longitudinal effect is believed to be relatively negligible in boundary layer analysis. So, in light of the applications, we explored the transverse curvature effect in this study. Chen and Mucoglu [15] discussed the importance of buoyancy in forced convective flow along a vertical cylinder for the first time. Employing the cubic spline interpolation method, Lee *et al.* [16] have investigated the combined convective effect on cylinder and needle. Heckel *et al.* [17] have explored slender cylinder with temperature variations of the surface. Transverse curvature effects on a slender cylinder were analysed by Wang and Klienstreuer [18]. The impact of rotation and time over a slender cylinder was explored in the study of Singh *et al.* [19]. The Nusselt number is more affected by localised cooling/heating than the skin friction coefficient, as evidenced by Kumari and Nath [20]. Aydin and Kaya [21] included MHD in their study over a slender cylinder and revealed that increasing the magnetic term enhances the heat transfer. Takhar *et al.* [22] found that velocity overshoot due to buoyancy forces in their study over a slender cylinder. Patil *et al.* [23,24] have worked on the slender cylinder by considering different effects like viscous dissipation, chemical reaction *etc*. Also, Rehman *et al.* [25] investigated the mixed convection stagnation point flow of Eyring–Powell fluid induced by an inclined cylindrical surface by considering Joule heating and magnetohydrodynamics (MHD).

Combined convective heat and mass transfer is now a common occurrence in various technical and natural systems. According to the second law of thermodynamics, entropy generation (EG) is linked to thermodynamic irreversibility. Entropy production occurs in all thermodynamic systems, and studying EG in a thermodynamical system can aid in improving the system's mechanical efficiency. A viscous fluid containing dissolved solute flows over the surface of a body, irreversible processes such as friction between fluid layers, thermal radiation, chemical reaction *etc*., occur. EG must be minimised to improve the efficiency of some technical systems, such as fuel cells, air separators, helical coils, microchannel, electro-chemicals, *etc*. The concept of EG was firstly proposed by Bejan [26]. Later, many researchers [5,27–36] have worked on this concept. However, finding the EG of a thermodynamical system to maximise work efficiency remains a significant and unavoidable challenge for researchers. Ahmed *et al.* [27] have focused their work on the effect of thermal stratification on EG. Khan *et al.* [28] explored the impact of EG between two rotating disks when bioconvection nanofluid flows between the disks. Khan *et al.* [29] reviewed the EG on the magnetised rotating hybrid nanoliquid flow amid two parallel plates. Recently, Haq *et al.* [30], Sahoo and Nandkeolyar [31], Khan *et al.* [5], Abbas *et al.* [32], Khan *et al.* [33], Shaw *et al.* [34], Afridi *et al.* [35,36] have worked on the concept of EG.

The difference in temperature between the ambient fluid and the wall does not have to be modest. A substantial difference in these temperatures significantly impacts the heat transfer [37,38] and fluid flow properties that determine the formed material sheet or fibre quality. To overcome this, one has to consider nonlinear (quadratic) temperature density differences in the buoyancy term of the momentum equation. A very few authors have worked on the nonlinear combined convection impact [39–42].

An examination of the literature reveals that no researchers have investigated the entropy generation effects over a slender cylinder in combination with nonlinear thermal radiation [31,42,43] and nonlinear combined convection. As a result, the current study's goals are centred on the following themes:

- Entropy generation analysis.
- Impact of nonlinear thermal radiation and combined quadratic convection on the profiles and gradients.
- Influence of time-dependent flow nature on the flow characteristics.
- Effect of liquid hydrogen and nitrogen diffusion.
- Impact of viscous dissipation on temperature profile and heat transfer rate.

Further, slender bodies find applications in the coating of wires, fibre sheets, optical fibres, photo electric devices, solar cells *etc*. In fact, thin wires in the shape of a slender cylinder must be cooled during such processes, and the energy and mass transport strengths must be managed to provide better outcomes. Also, liquid hydrogen and liquid nitrogen act as a better cooling agent. In such modelling processes entropy generation occurs, and studying EG in a thermodynamical system can aid in improving the system's mechanical efficiency.

2. Mathematical Formulation

A two-dimensional axisymmetric time-dependent triple diffusive quadratic combined convective flow over a slender cylinder with nonlinear thermal radiation and entropy generation is investigated in this work. The vertical axis of the slender cylindrical wall is used to measure the axial coordinate x, and the radial coordinate r is measured using the cylinder's axis as the starting point. The orifice from which the narrow cylinder emerges is referred to as Origin O. The water is used as the base fluid and liquid hydrogen and nitrogen serving as diffusion components. The radius r_0 of the slender cylinder is equal to the order of the thickness of the boundary layer. In the momentum balance equation, the density variations are accounted for only in the buoyancy term by virtue of the Boussinesq approximation [44,45]. The temperature of the cylinder's wall is T_w, while, T_∞ is the ambient fluid temperature. Further, C_1, C_2 are the species concentration of liquid hydrogen and nitrogen. Also, C_{1w}, C_{2w} and $C_{1\infty}$, $C_{2\infty}$ are the species concentration at the wall and ambient fluid. Here we assumed that $T_w > T_\infty$, $C_{1w} > C_{1\infty}$, $C_{2w} > C_{2\infty}$. Fig. 1 illustrates the flow geometry of the current problem. The following equations govern the unsteady boundary layer flow around a slender cylinder [4,19,22,23].

$$\frac{\partial(ru)}{\partial x} + \frac{\partial(rv)}{\partial r} = 0 \tag{1}$$

$$\begin{aligned}\frac{\partial u}{\partial t} + u\frac{\partial u}{\partial x} + v\frac{\partial u}{\partial r} &= \frac{\partial U_e}{\partial t} + \frac{v}{r}\frac{\partial}{\partial r}\left(r\frac{\partial u}{\partial r}\right)\\ &+g\left[\beta_1(T-T_\infty)+\beta_2(T-T_\infty)^2+\cdots\right]\\ &+g\left[\beta_3(C_1-C_{1\infty})+\beta_4(C_1-C_{1\infty})^2+\cdots\right]\\ &+g\left[\beta_5(C_2-C_{2\infty})+\beta_6(C_2-C_{2\infty})^2+\cdots\right]\end{aligned} \tag{2}$$

$$\frac{\partial T}{\partial t} + u\frac{\partial T}{\partial x} + v\frac{\partial T}{\partial r} = \frac{\alpha}{r}\frac{\partial}{\partial r}\left(r\frac{\partial T}{\partial r}\right) - \frac{1}{\rho C_p}\frac{\partial q_r}{\partial r} + \frac{v}{C_p}\left(\frac{\partial u}{\partial r}\right)^2 \tag{3}$$

$$\frac{\partial C_1}{\partial t} + u\frac{\partial C_1}{\partial x} + v\frac{\partial C_1}{\partial r} = \frac{D_{S_1}}{r}\frac{\partial}{\partial r}\left(r\frac{\partial C_1}{\partial r}\right) \tag{4}$$

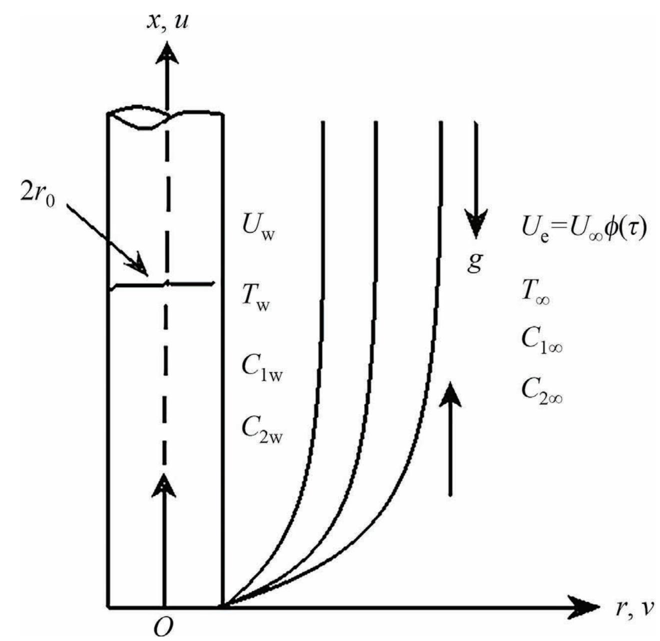

Fig. 1. Flow geometry of the current physical problem.

$$\frac{\partial C_2}{\partial t}+u\frac{\partial C_2}{\partial x}+v\frac{\partial C_2}{\partial r}=\frac{D_{S_2}}{r}\frac{\partial}{\partial r}\left(r\frac{\partial C_2}{\partial r}\right) \tag{5}$$

The initial conditions of the problem are:

$$\begin{aligned}&u(x,r,0)=u_i(x,r),v(x,r,0)=v_i(x,r),T(x,r,0)=T_i(x,r)\\&C_1(x,r,0)=C_{1i}(x,r),C_2(x,r,0)=C_{2i}(x,r)\end{aligned} \tag{6}$$

The corresponding boundary constraints are:

$$\left.\begin{aligned}&\text{At } r=r_0: \ u(x,\ r_0,\ t)=0,\quad v(x,\ r_0,\ t)=v_{\rm w},\\&T(x,\ r_0,\ t)=T_{\rm w},\ C_1(x,\ r_0,\ t)=C_{1\rm w},\\&C_2(x,\ r_0,\ t)=C_{2\rm w}\\&\text{As } r\to\infty: \ u(x,\ \infty,\ t)\to U_{\rm e}=U_\infty\phi(\tau),\\&T(x,\ \infty,\ t)\to T_\infty,\\&C_1(x,\ \infty,\ t)\to C_{1\infty},\ C_2(x,\ \infty,\ t)\to C_{2\infty}\end{aligned}\right\} \tag{7}$$

The non-similar transformations given below are utilised to nondimensionalize the Eqs. (2)–(5) and define the stream function ψ that satisfies the equation of continuity (1):

$$\xi=\left(\frac{4}{r_0}\right)\left(\frac{\nu x}{U_\infty}\right)^{1/2},\ \eta=\left(\frac{U_\infty}{\nu x}\right)^{1/2}\left[\frac{r^2-r_0^2}{4r_0}\right],\tau=\frac{\nu t}{r_0^2},$$

$$\frac{r^2}{r_0^2}=(1+\xi\eta),\ G=\frac{T-T_\infty}{T_{\rm w}-T_\infty},\ H=\frac{C_1-C_{1\infty}}{C_{1\rm w}-C_{1\infty}}$$

$$S=\frac{C_2-C_{2\infty}}{C_{2\rm w}-C_{2\infty}},\ q_r=-\left(\frac{16\sigma^*T^3}{3k^*}\right)\frac{\partial T}{\partial r}.$$

$\psi(x,r,t)=r_0(\nu U_\infty x)^{1/2}\phi(\tau)f(\xi,\eta,\tau)$,$F=f_\eta$, where $\phi(\tau)=1+\alpha\tau^2$, and $u=\frac{\partial\psi}{\partial y},\ v=-\frac{\partial\psi}{\partial x}$.

Therefore,

$u=\frac{1}{2}U_{\rm e}F$, where $U_{\rm e}=U_\infty\phi(\tau)$ and $v=\frac{r_0}{2r}\left(\frac{\nu U_\infty}{x}\right)^{1/2}\phi(\tau)\{\eta F-f-\xi f_\xi\}$.

Thus, the transformed nondimensional equations are:

$$\begin{aligned}&(1+\xi\eta)F_{\eta\eta}+\left(\xi+\phi f+\xi\phi f_\xi\right)F_\eta+\frac{\xi^2}{4}\left[(2-F)\phi^{-1}\frac{{\rm d}\phi}{{\rm d}\tau}-F_\tau\right]\\&-\xi\phi FF_\xi+8Ri\ \phi^{-1}G(1+\beta_tG)+8Ri\ \phi^{-1}Nc_1H\left(1+\beta_{c_1}H\right)\\&+8Ri\ \phi^{-1}Nc_2S\left(1+\beta_{c_2}S\right)=0\end{aligned} \tag{8}$$

$$\begin{aligned}&(1+\xi\eta)G_{\eta\eta}+\left(\frac{\xi}{2}+\frac{\xi}{2P}+\frac{Pr\phi f}{P}+\frac{Pr\xi\phi f_\xi}{P}\right)G_\eta-\frac{Pr\xi^2}{4P}G_\tau\\&-\frac{Pr\xi\phi FG_\xi}{P}+\frac{3R_{\rm d}(\theta_{\rm w}-1)(1+\xi\eta)Q^2}{P}G_\eta^2+\frac{PrEc\ \phi^2(1+\xi\eta)F_\eta^2}{P}\\&=0\end{aligned} \tag{9}$$

$$(1+\xi\eta)H_{\eta\eta}+\left(\xi+Sc_1\phi f+Sc_1\xi\phi f_\xi\right)H_\eta-Sc_1\xi\phi FH_\xi-\frac{Sc_1}{4}\xi^2H_\tau=0 \tag{10}$$

$$(1+\xi\eta)S_{\eta\eta}+\left(\xi+Sc_2\phi f+Sc_2\xi\phi f_\xi\right)S_\eta-Sc_2\xi\phi FS_\xi-\frac{Sc_2}{4}\xi^2S_\tau=0 \tag{11}$$

and the pertinent nondimensional boundary constraints are:

$$\left.\begin{aligned}&\text{At }\ \eta=0\ \ :\ F(\xi,0,\tau)=0,\quad G(\xi,0,\tau)=1,\\&\qquad H(\xi,0,\tau)=1,\quad S(\xi,0,\tau)=1\\&\text{As }\eta\to\infty\ \ :\ F(\xi,\infty,\tau)\to2,\ \ G(\xi,\infty,\tau)\to0,\\&\qquad H(\xi,\infty,\tau)\to0,\ \ S(\xi,\infty,\tau)\to0\end{aligned}\right\} \tag{12}$$

where, $Gr=\frac{g\beta_1(T_{\rm w}-T_\infty)x^3}{\nu^2}$,$Re_x=\frac{U_\infty x}{\nu}$,$Ri=\frac{Gr}{Re_x^2}$,

$$\begin{aligned}&\beta_t=\frac{\beta_2}{\beta_1}(T_{\rm w}-T_\infty),\ \beta_{c_1}=\frac{\beta_4}{\beta_3}(C_{1\rm w}-C_{1\infty}),\ \beta_{c_2}=\frac{\beta_6}{\beta_5}(C_{2\rm w}-C_{2\infty}),\\&Nc_1=\frac{\beta_3(C_{1\rm w}-C_{1\infty})}{\beta_1(T_{\rm w}-T_\infty)},\ Nc_2=\frac{\beta_5(C_{2\rm w}-C_{2\infty})}{\beta_1(T_{\rm w}-T_\infty)},\ Pr=\tfrac{\nu}{\alpha},\\&R_{\rm d}=\frac{16\sigma^*T_\infty^3}{3k^*k},\ \theta_{\rm w}=\frac{T_{\rm w}}{T_\infty},\ Q=1+(\theta_{\rm w}-1)G,\\&P=\left(1+R_{\rm d}Q^3\right),\ Sc_1=\frac{\nu}{D_{s_1}},\ Sc_2=\frac{\nu}{D_{s_2}},\ Ec=\frac{U_\infty^2}{C_p(T_{\rm w}-T_\infty)}.\end{aligned}$$

Here, $f(\xi,\eta,\tau)=\int_0^\eta F{\rm d}\eta+f_{\rm w}$ and $f_{\rm w}$ can be obtained from $v=\frac{r_0}{2r}\left(\frac{\nu U_\infty}{x}\right)^{1/2}\phi(\tau)\{\eta F-f-\xi f_\xi\}$.

Using the boundary condition $v=v_{\rm w}$ at $\eta=0$ from Eq. (7), $v_{\rm w}=-\frac{1}{2}\left(\frac{\nu U_\infty}{x}\right)\phi\left[f_{\rm w}+\xi(f_\xi)_{\rm w}\right]$ after the simplification we get, $f_{\rm w}(\xi,0,\tau)=A\phi^{-1}\xi$, where $A=\frac{-v_{\rm w}r_0}{2\nu}$.

The fluid friction at the surface of the slender cylinder, the energy transfer rate and mass transfer rates at the slender cylinder wall to the ambient fluid are given by the Eqs. (13)–(16), respectively.

$$Re_x^{1/2}C_f=\frac{1}{2}\phi F_\eta(\xi,0,\tau) \tag{13}$$

$$Nu\ Re_x^{-1/2}=-\frac{1}{2}\left(1+R_{\rm d}(1+(\theta_{\rm w}-1)G)^3\right)G_\eta(\xi,0,\tau) \tag{14}$$

$$Sh_1Re_x^{-1/2}=-\frac{1}{2}H_\eta(\xi,0,\tau) \tag{15}$$

$$Sh_2Re_x^{-1/2}=-\frac{1}{2}S_\eta(\xi,0,\tau) \tag{16}$$

3. Entropy Generation

The entropy model for the present problem can be written as [5,33–36]:

HTI (heat transfer irreversibility) is the local EG due to heat transfer. Due to the Joule effect and fluid friction, the EG is summed

$$E_{\text{gen}}=\underbrace{\frac{1}{T^2}\left[k\left(\frac{\partial T}{\partial r}\right)^2+\frac{16\sigma^*T^3}{3k^*}\left(\frac{\partial T}{\partial r}\right)^2\right]}_{\text{HTI}}+\underbrace{\left[\frac{\mu}{T}\left(\frac{\partial u}{\partial r}\right)^2\right]}_{\text{FFI}}$$

$$+\underbrace{\left[\frac{R^*D_{s_1}}{C_{1\infty}}\left(\frac{\partial C_1}{\partial r}\right)^2+\frac{R^*D_{s_1}}{T_\infty}\left(\frac{\partial C_1}{\partial r}\frac{\partial T}{\partial r}\right)+\frac{R^*D_{s_2}}{C_{2\infty}}\left(\frac{\partial C_2}{\partial r}\right)^2+\frac{R^*D_{s_2}}{T_\infty}\left(\frac{\partial C_2}{\partial r}\frac{\partial T}{\partial r}\right)+\frac{R^*D_{s_{12}}}{C_{2\infty}}\left(\frac{\partial C_1}{\partial r}\frac{\partial C_2}{\partial r}\right)\right]}_{\text{DI}}$$

up as FFI (fluid friction irreversibility). DI is diffusion irreversibility due to species concentration and temperature. Using the characteristic entropy rate $E_0=\frac{\Delta T^2 k}{T_\infty^2 x^2}$, the local E_{gen} is nondimensionalized (E_{G}).

$$E_{\text{G}}=\frac{E_{\text{gen}}}{E_0}=N_1+N_2+N_3$$

where, $N_1=\frac{\text{HTI}}{E_0}=\frac{(1+\xi\eta)}{4(1+\Omega_{\text{T}}G)^2}Re_x(1+R_{\text{d}}P)G_\eta^2$,

$$N_2=\frac{\text{FFI}}{E_0}=\frac{BrRe_x(1+\xi\eta)}{16(1+\Omega_{\text{T}}G)\Omega_{\text{T}}}\phi^2F_\eta^2,$$

$$\begin{aligned}N_3&=\frac{\text{DI}}{E_0}\\&=\frac{M_1}{4}\frac{\Omega_{c_1}(1+\xi\eta)Re_x}{\Omega_{\text{T}}}H_\eta\left(\frac{\Omega_{c_1}}{\Omega_{\text{T}}}H_\eta+G_\eta\right)+\frac{M_2}{4}\\&\times\frac{\Omega_{c_2}(1+\xi\eta)Re_x}{\Omega_{\text{T}}}S_\eta\left(\frac{\Omega_{c_2}}{\Omega_{\text{T}}}S_\eta+G_\eta\right)+\frac{M_3}{4}\frac{\Omega_{c_2}^2(1+\xi\eta)Re_x}{\Omega_{\text{T}}^2}H_\eta S_\eta.\end{aligned}$$

where, $M_1=\frac{R^*D_{s_1}C_{1\infty}}{k}$, $M_2=\frac{R^*D_{s_2}C_{2\infty}}{k}$, $M_3=\frac{R^*D_{s_{12}}C_{1\infty}}{k}$, $\Omega_{\text{T}}=\frac{\Delta T}{T_\infty}$, $\Omega_{c_1}=\frac{\Delta C_1}{C_{1\infty}}$, $\Omega_{c_2}=\frac{\Delta C_2}{C_{2\infty}}$, $Pr=\frac{\nu}{\alpha}$, $Ec=\frac{U_\infty^2}{C_p\Delta T}$, $Br=Pr\ Ec$, $Q=[1+(\theta_{\text{w}}-1)G]$ and $P=\left(1+R_{\text{d}}Q^3\right)$.

And Bejan number is mathematically defined as,

$$\text{Bejan Number}, Be=\frac{\text{HTI}}{E_{\text{G}}}=\frac{N_1}{N_1+N_2+N_3}=\frac{\text{Irreversibility due to heat transfer}}{\text{Total local entropy}}$$

which indicates the contribution of entropy generated due to heat transfer relative to the total entropy generated.

4. Numerical Procedure

The method of quasilinearization [9,46,47] is employed to linearize the Eqs. (8)–(11), which is then followed by the implicit finite difference scheme [48–50] to discretize the resulting equations.

$$F_{\eta\eta}^{i+1}+A_1^iF_\eta^{i+1}+A_2^iF_\xi^{i+1}+A_3^iF_\tau^{i+1}+A_4^iF^{i+1}+A_5^iG^{i+1}+A_6^iH^{i+1}+A_7^iS^{i+1}=A_8^i \quad (17)$$

$$G_{\eta\eta}^{i+1}+B_1^iG_\eta^{i+1}+B_2^iG_\xi^{i+1}+B_3^iG_\tau^{i+1}+B_4^iG^{i+1}+B_5^iF^{i+1}+B_6^iF_\eta^{i+1}=B_7^i \quad (18)$$

$$H_{\eta\eta}^{i+1}+C_1^iH_\eta^{i+1}+C_2^iH_\xi^{i+1}+C_3^iH_\tau^{i+1}+C_4^iF^{i+1}=C_5^i \quad (19)$$

$$S_{\eta\eta}^{i+1}+D_1^iS_\eta^{i+1}+D_2^iS_\xi^{i+1}+D_3^iS_\tau^{i+1}+D_4^iF^{i+1}=D_5^i \quad (20)$$

The equivalent boundary conditions are:

$$\left.\begin{array}{lllll}\text{At } \eta=0 & : F^{i+1}=0, & G^{i+1}=1, & H^{i+1}=1, & S^{i+1}=1\\ \text{As } \eta=\eta_\infty & : F^{i+1}=2, & G^{i+1}=0, & H^{i+1}=0, & S^{i+1}=0\end{array}\right\} \quad (21)$$

The solution of the so obtained set of linear equations with its coefficient matrix in the block tri-diagonal form is computed by applying Varga's algorithm [51]. The results iteratively converge to the solution with a precision of 10^{-4}. *i.e.*,

$$\text{Max}\left\{\left|(F_\eta)_{\text{w}}^{i+1}-(F_\eta)_{\text{w}}^{i}\right|,\left|(G_\eta)_{\text{w}}^{i+1}-(G_\eta)_{\text{w}}^{i}\right|,\left|(H_\eta)_{\text{w}}^{i+1}-(H_\eta)_{\text{w}}^{i}\right|,\left|(S_\eta)_{\text{w}}^{i+1}-(S_\eta)_{\text{w}}^{i}\right|\right\}\leqslant 10^{-4}.$$

The coefficients of Eqs. (17)–(20) are:

$$A_1^i=\frac{\xi+\phi f+\xi\phi f_\xi}{1+\xi\eta}, A_2^i=\frac{-\xi\phi F}{1+\xi\eta}, A_3^i=\frac{-\xi^2}{4(1+\xi\eta)},$$

$$A_4^i=\frac{-1}{1+\xi\eta}\left(\frac{\xi^2}{4}\phi^{-1}\phi_\tau+\xi\phi F_\xi\right), A_5^i=\frac{8}{1+\xi\eta}Ri\phi^{-1}(1+2\beta_tG),$$

$$A_6^i=\frac{8}{1+\xi\eta}Ri\phi^{-1}Nc_1(1+2\beta_{c_1}H),$$

$$A_7^i=\frac{8}{1+\xi\eta}Ri\phi^{-1}Nc_2(1+2\beta_{c_2}S),$$

$$A_8^i=2A_3^i\phi^{-1}\phi_\tau+A_2^iF_\xi+\tfrac{8}{1+\xi\eta}Ri\phi^{-1}\left(\beta_tG^2+Nc_1\beta_{c_1}H^2+Nc_2\beta_{c_2}S^2\right),$$

$$B_1^i=\left[\frac{1}{1+\xi\eta}\left(\frac{\xi}{2}+\frac{\xi}{2P}+\frac{Pr\phi f}{P}+\frac{Pr\phi\xi f_\xi}{P}\right)+\frac{6R_{\text{d}}(\theta_{\text{w}}-1)Q^2}{P}G_\eta\right],$$

$$B_2^i=-\frac{Pr\ \phi\xi F}{P(1+\xi\eta)}, B_3^i=-\frac{Pr\ \xi^2}{4P(1+\xi\eta)},$$

$$B_4^i=\left[-\left(\left(\frac{\xi}{2}+Pr\ \phi f+Pr\phi\xi f_\xi\right)-\frac{Pr\ \xi^2G_\tau}{4}-Pr\ \xi\phi FG_\xi\right)\right.$$
$$\left(\frac{3R_{\text{d}}(\theta_{\text{w}}-1)Q^2}{P^2(1+\xi\eta)}\right)+3R_{\text{d}}(\theta_{\text{w}}-1)^2Q\left(\frac{2P-3R_{\text{d}}Q^3}{P^2}\right)$$

Table 1
Comparison of the present steady-state results ($F_\eta(\xi,0)$,$G_\eta(\xi,0)$) with earlier published results

ξ	Ri	Roy and Anilkumar [4]		Singh *et al.* [19]		Takhar *et al.* [22]		Present results	
		$F_\eta(\xi,0)$	$G_\eta(\xi,0)$	$F_\eta(\xi,0)$	$G_\eta(\xi,0)$	$F_\eta(\xi,0)$	$G_\eta(\xi,0)$	$F_\eta(\xi,0)$	$G_\eta(\xi,0)$
0	0	1.3282	0.5854	1.3281	0.5854	1.3281	0.5854	1.3280	0.5455
0	1	4.9664	0.8220	4.9663	0.8219	4.9665	0.8221	4.9665	0.8220
0	2	7.7122	0.9304	7.7119	0.9302	7.7124	0.9303	7.7121	0.9302
1	0	1.9169	0.8666	1.9167	0.8666	1.9168	0.8668	1.9167	0.8667
1	1	5.2580	1.0621	5.2578	1.0617	5.2580	1.0618	5.2579	1.0618
1	2	7.8871	1.1688	7.8863	1.1685	7.8870	1.1692	7.8868	1.1688

$$G_\eta^2 + Pr\,Ec\,\phi^2 F_\eta^2 \left(\frac{3R_\mathrm{d}(\theta_\mathrm{w}-1)Q^2}{P^2}\right)\Bigg]$$

$$B_5^i = -\frac{Pr\,\xi\phi G_\xi}{P(1+\xi\eta)},\ B_6^i = \frac{2Pr\,Ec\,\phi^2 F_\eta}{P},\ B_7^i = \frac{3R_\mathrm{d}(\theta_\mathrm{w}-1)Q^2}{P}$$

$$G_\eta^2 + B_2^i G_\xi + B_4^i G + \tfrac{B_6^i}{2} F_\eta$$

$$C_1^i = \frac{1}{1+\xi\eta}\left(\xi + Sc_1\phi f + Sc_1\phi\xi f_\xi\right),\ C_2^i = -\frac{Sc_1\xi\phi F}{1+\xi\eta},$$

$$C_3^i = -\frac{Sc_1\xi^2}{4(1+\xi\eta)},$$

$$C_4^i = -\frac{Sc_1\xi\phi H_\xi}{4(1+\xi\eta)},\ C_5^i = C_4^i F,$$

$$D_1^i = \frac{1}{1+\xi\eta}\left(\xi + Sc_2\phi f + Sc_2\phi\xi f_\xi\right),$$

$$D_2^i = -\frac{Sc_2\xi\phi F}{1+\xi\eta},\ D_3^i = -\frac{Sc_2\xi^2}{4(1+\xi\eta)},$$

$$D_4^i = -\frac{Sc_2\xi\phi S_\xi}{4(1+\xi\eta)},\ D_5^i = D_4^i F.$$

In order to validate the authentication of the accuracy of the results of the present analysis, the present results of gradients are compared with the previous research findings of Roy and Anilkumar [4], Singh *et al.* [19] and Takhar *et al.* [22] in Table 1, which shows that the current findings are consistent with the results obtained in [4],[19] and [22].

5. Results and Discussion

The ranges of values of several parameters considered in this study are as follows: $-1 \leqslant Ri \leqslant 10$, $-1 \leqslant A \leqslant 1$, $0 \leqslant \tau \leqslant 1$, $1.5 \leqslant \theta_\mathrm{w} \leqslant 2.0$, $0 \leqslant R_\mathrm{d} \leqslant 2$, $-0.5 \leqslant \alpha \leqslant 0.5$, $0 \leqslant \xi \leqslant 0.5$, $0.5 \leqslant \Omega_\mathrm{T} \leqslant 2.0$. Also, some parameter values are kept constant *i. e.*, Pr = 7 (water), $Sc_1 = 160$ (liquid hydrogen), $Sc_2 = 240$ (liquid nitrogen) [52].

5.1. Effect of linear and quadratic combined convection parameter

The significance of the impact of linear and quadratic combined convection parameters and time is structured in Figs. 2–5 on the fluid velocity, temperature, local friction coefficient at the surface, and the local energy transfer rate. The profiles are drawn for accelerating flow $\phi(\tau) = 1 + \alpha\tau^2$, $\alpha = 0.5$ and the corresponding gradients are drawn for both accelerating ($\alpha > 0$) and decelerating

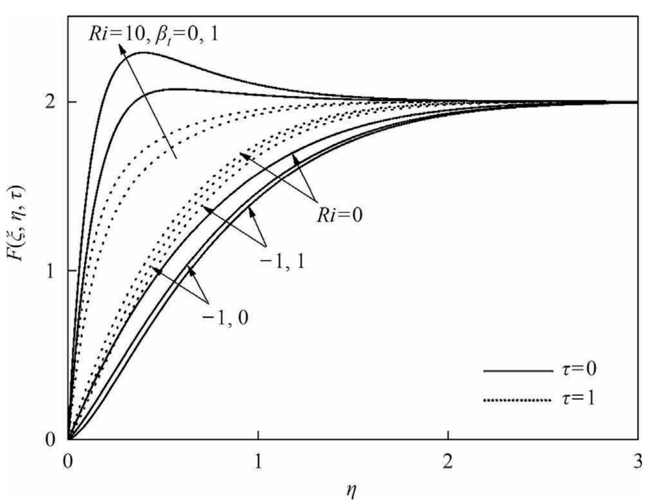

Fig. 2. Variation of velocity $F(\xi,\eta,\tau)$ for $\phi(\tau) = 1 + \alpha\tau^2$, $\alpha = 0.5$ for different values of Ri and β_t when $\theta_\mathrm{w} = 1.5$, $A = 1$, $\beta_{c_1} = \beta_{c_1} = Nc_1 = Nc_2 = R_\mathrm{d} = 0.1$ and $\xi = 0.5$.

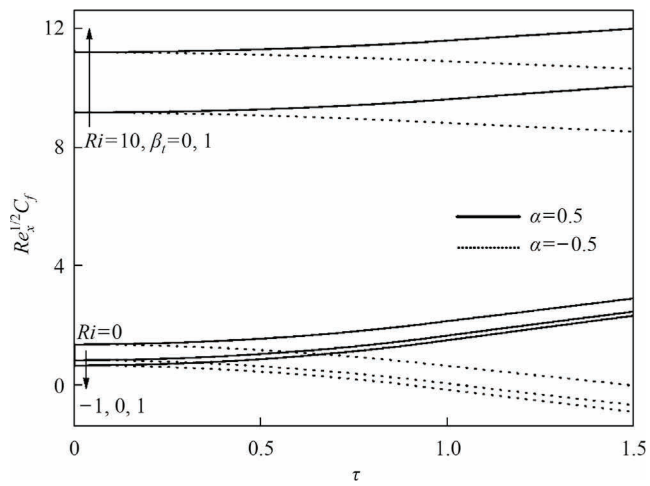

Fig. 3. Variation of local surface friction coefficient for different values of Ri and β_t when $\theta_\mathrm{w} = 1.5$, $A = 1$, $\beta_{c_1} = \beta_{c_1} = Nc_1 = Nc_2 = R_\mathrm{d} = 0.1$ and $\xi = 0.5$.

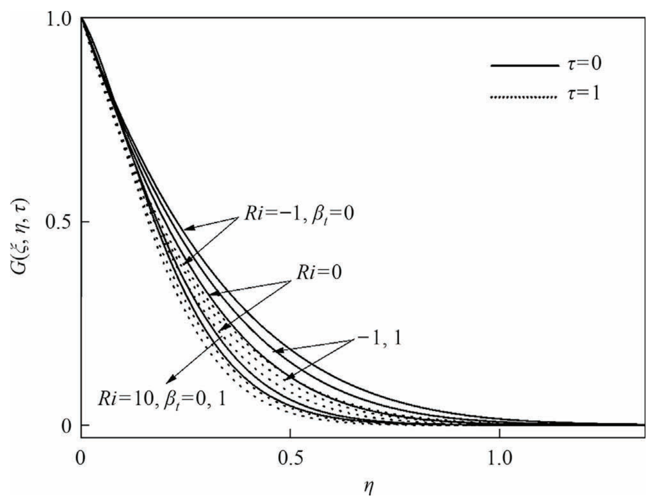

Fig. 4. Variation of temperature $G(\xi,\eta,\tau)$ for $\phi(\tau) = 1 + \alpha\tau^2$, $\alpha = 0.5$ for different values of Ri and β_t when $\theta_\mathrm{w} = 1.5$, $A = 1$, $\beta_{c_1} = \beta_{c_1} = Nc_1 = Nc_2 = R_\mathrm{d} = 0.1$ and $\xi = 0.5$.

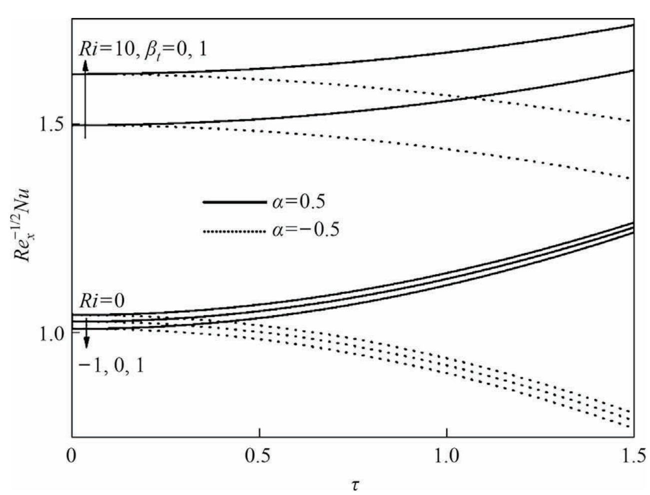

Fig. 5. Variation of local Nusselt number $Re_x^{-1/2}Nu$ for different values of Ri and β_t when $\theta_\mathrm{w} = 1.5$, $A = 1$, $\beta_{c_1} = \beta_{c_1} = Nc_1 = Nc_2 = R_\mathrm{d} = 0.1$ and $\xi = 0.5$.

($\alpha < 0$) flows. The fluid velocity (F), local friction coefficient at the surface ($Re_x^{1/2}C_f$), and the local energy transfer rate ($Re_x^{-1/2}Nu$) enhance for quadratic combined convection parameter ($\beta_t = 1$) when compared to the linear combined convection parameter ($\beta_t = 0$) while the fluid temperature (G) declines in the case of aiding buoyancy flow ($Ri > 0$) for both time-dependent and independent flows, which is justified by the fact that higher values of β_t causes very intense convection of the fluid particles due to the larger temperature difference. The reverse pattern is found in the case of opposing buoyancy flow ($Ri < 0$). On the other hand, the quadratic combined convection parameter β_t has no effect when $Ri = 0$ as it signifies the forced convection flow. Also, decrement in the fluid velocity and temperature can be seen in Figs. 2 and 4 as time surge when $Ri > 0$.

Further, Ri upsurges the fluid velocity, local friction factor, and thermal efficiency by reducing the temperature of the fluid as it functions as a positive pressure gradient. It is clear from Figs. 3 and 5 that as time surges, the gradients at the surface augment for accelerating flow ($\alpha > 0$) and decline for decelerating flow ($\alpha < 0$). Particularly, the local energy transport strength and friction coefficient at the surface enhance approximately 50% and 87%, respectively, when Ri increments from −1 to 10 at $\tau = 1$, $\beta_t = 1$ and $\alpha = 0.5$.

5.2. Effect of surface mass transfer and streamwise coordinate

Figs. 6 and 7 describe the influence of the surface mass transfer constraint (A) along with the streamwise coordinate ξ and time τ on the temperature profile and the corresponding gradient. The values $\xi \neq 0$ and $\xi = 0$ indicate the non-similarity and similarity solutions, respectively. Since streamwise coordinates behave as a negative pressure gradient, the temperature G of the fluid diminishes in case of suction ($A > 0$) for both $\tau = 0$, $\tau \neq 0$ while energy transport strength enhances. At the same time, the contrary outcomes are observed for injection ($A < 0$). The fluid temperature is more and energy transport strength is less for the permeable surface ($A \neq 0$) when compared with the impermeable surface ($A = 0$) in case of injection ($A < 0$). This is because fluid injection moves the fluid particles from the hotter region near the wall to the colder region away from the surface. Whereas in the case of suction ($A > 0$), quite reverse results are obtained. Specifically, the energy transport strength is approximately 140% more for

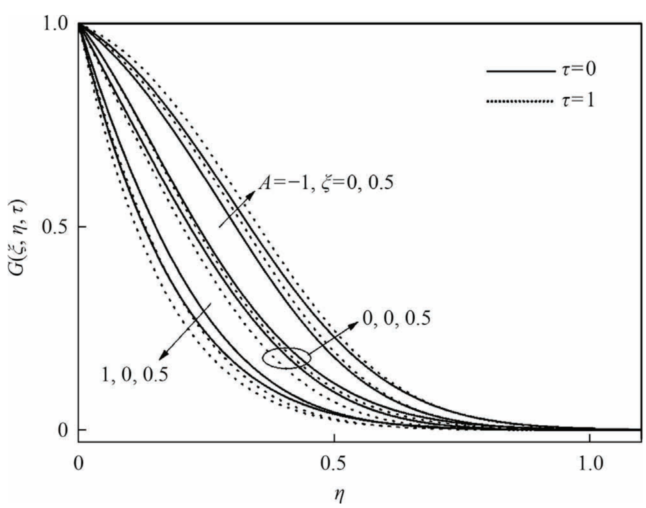

Fig. 6. Variation of temperature $G(\xi,\eta,\tau)$ for $\phi(\tau) = 1 + \alpha\tau^2$, $\alpha = 0.5$ for different values of A and ξ when $\theta_w = 1.5$, $Ri = 10$ and $\beta_t = \beta_{c_1} = \beta_{c_1} = Nc_1 = Nc_2 = R_d = 0.1$.

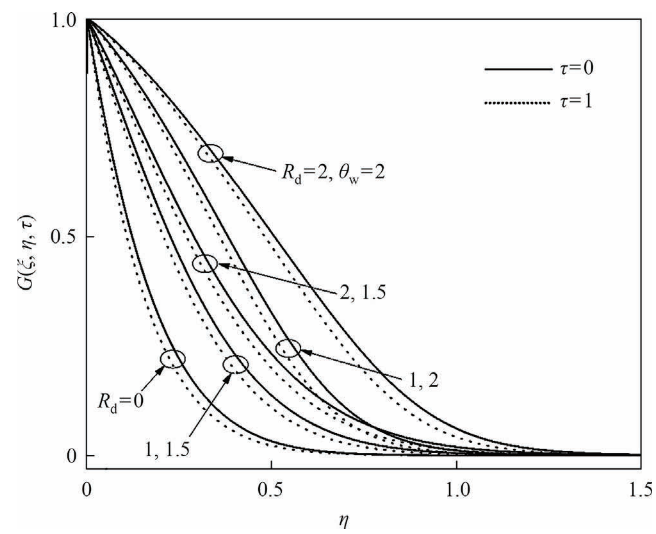

Fig. 8. Variation of temperature $G(\xi,\eta,\tau)$ for $\phi(\tau) = 1 + \alpha\tau^2$, $\alpha = 0.5$ for different values of R_d and θ_w when $A = 1$, $Ri = 10$, $\beta_t = \beta_{c_1} = \beta_{c_1} = Nc_1 = Nc_2 = 0.1$ and $\xi = 0.5$.

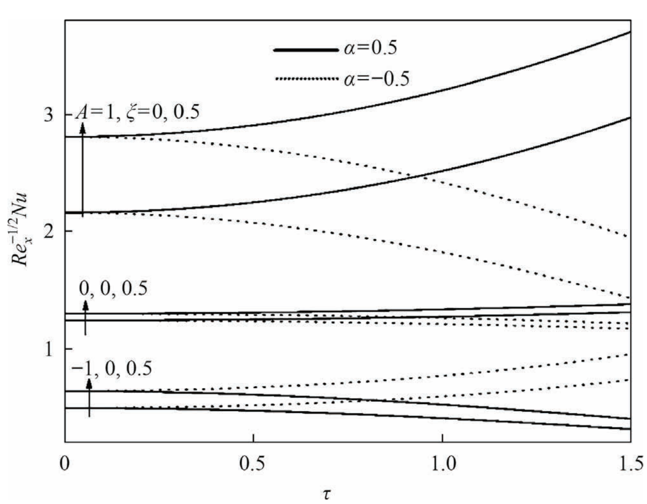

Fig. 7. Variation of $Re_x^{-1/2}Nu$ for different values of A and ξ when $\theta_w = 1.5$, $Ri = 10$, $\beta_t = \beta_{c_1} = \beta_{c_1} = Nc_1 = Nc_2 = R_d = 0.1$ and $\xi = 0.5$.

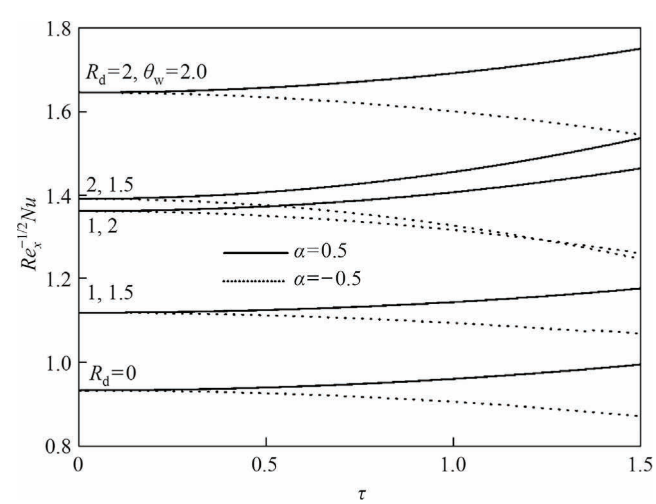

Fig. 9. Variation of $Re_x^{-1/2}Nu$ for different values of R_d and θ_w when $A = 1$, $Ri = 10$, $\beta_t = \beta_{c_1} = \beta_{c_1} = Nc_1 = Nc_2 = 0.1$ and $\xi = 0.5$.

the permeable surface thanthe impermeable one, in case of suction at $\tau = 1$ when $\xi = 0.5$, $\alpha = 0.5$.

5.3. Effect of nonlinear thermal radiation

The variation of temperature profile and local energy transport strength for different values of radiation parameter R_d, temperature ratio parameter θ_w, and time τ are addressed in Figs. 8 and 9, where $R_d = 0$ corresponds to no thermal radiation. The enhancing values of R_d and θ_w augments the fluid temperature for both $\tau = 0$ and $\tau \neq 0$, and local Nusselt number. Because, the fluid absorbs the heat energy released due to radiation R_d, and in turn releases the heat energy from the cylinder to the surrounding surface, resulting in increase in both temperature of the fluid and rate of heat transfer. Also, θ_w is the ratio of temperature at the wall and ambient temperature, is always greater than 1. Hence, augmentation in the values of θ_w augments the fluid temperature and the energy transport strength. Further, it is noticed from Fig. 9 that the $Re_x^{-1/2}Nu$ augments for accelerating flow ($\alpha > 0$) and declines for decelerating flow ($\alpha < 0$). When comparing the nonlinear thermal radiation withthe non-radiation case, the local Nusselt number is enhanced by around 18% at $\tau = 1$, $R_d = 1$, $\theta_w = 1.5$, $\alpha = 0.5$. The temperature ratio attribute θ_w designates the thermal state of the fluid.

5.4. Effect of diffusing components

Figs. 10 and 11 exemplify the effect of time and surface mass transfer attribute A on species concentration profiles and the corresponding mass transfer rates. The species concentration profiles decrease, and the mass transfer rate upsurges for the permeable surface ($A > 0$) compared with the impervious surface ($A = 0$). Also, the species concentration profiles decline as time emerges. Furthermore, from Figs. 10 and 11, we noticed that liquid hydrogen diffusion has a larger magnitude of species concentration profile than liquid nitrogen diffusion. However, liquid nitrogen diffusion has a greater mass transfer rate than liquid hydrogen. For instance, the mass transfer strength of liquid nitrogen is about 44% more than that of liquid hydrogen at $\tau = 1$ when $\alpha = 0.5$, $A = 0.5$. *i.e.*, liquid nitrogen is a better coolant than liquid hydrogen.

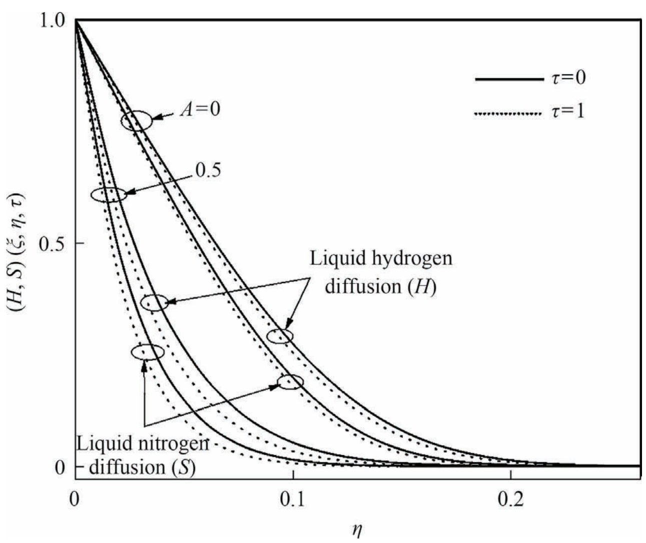

Fig. 10. Variation of $(H,S)(\xi,\eta,\tau)$ for $\phi(\tau) = 1 + \alpha\tau^2$, $\alpha = 0.5$ for different values of A when $\theta_w = 1.5$, $Ri = 10$, $\beta_t = \beta_{c_1} = \beta_{c_1} = Nc_1 = Nc_2 = R_d = 0.1$ and $\xi = 0.5$.

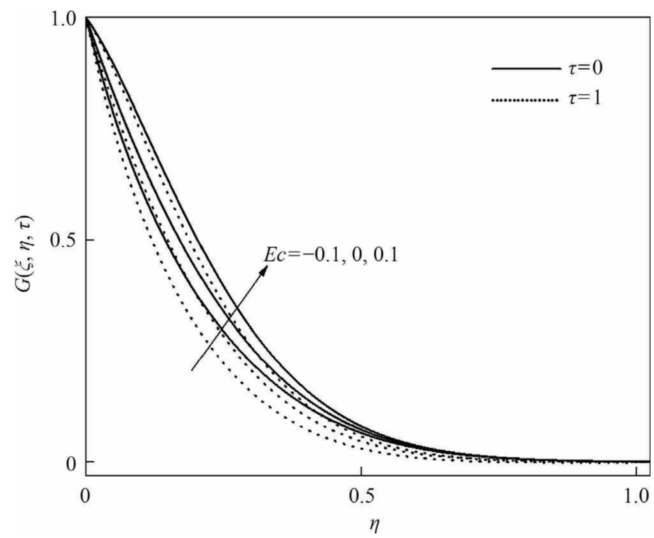

Fig. 12. Variation of temperature $G(\xi,\eta,\tau)$ for $\phi(\tau) = 1 + \alpha\tau^2$, $\alpha = 0.5$ for different values of Ec when $\theta_w = 1.5$, $A = 1$, $Ri = 10$, $\beta_t = \beta_{c_1} = \beta_{c_1} = Nc_1 = Nc_2 = R_d = 0.1$ and $\xi = 0.5$.

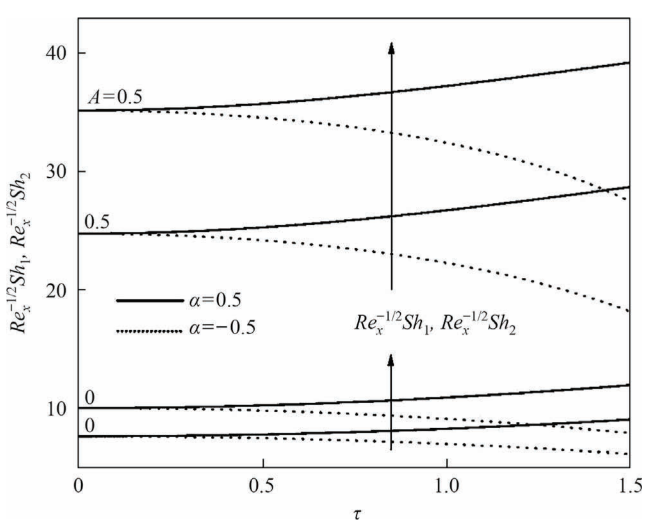

Fig. 11. Effect of A on mass transfer rates $Re_x^{1/2}Sh_1$ and $Re_x^{1/2}Sh_2$ when $\theta_w = 1.5$, $Ri = 10$, $\beta_t = \beta_{c_1} = \beta_{c_1} = Nc_1 = Nc_2 = R_d = 0.1$ and $\xi = 0.5$.

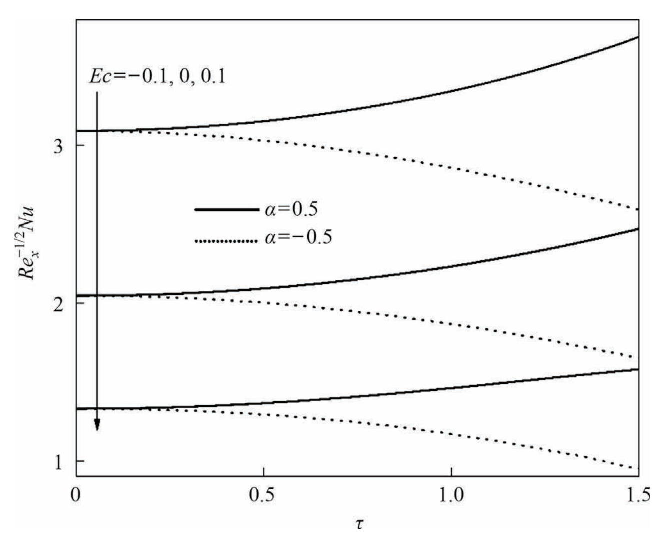

Fig. 13. Variation of $Re_x^{-1/2}Nu$ for different values of Ec when $\theta_w = 1.5$, $A = 1$, $Ri = 10$, $\beta_t = \beta_{c_1} = \beta_{c_1} = Nc_1 = Nc_2 = R_d = 0.1$ and $\xi = 0.5$.

5.5. Effect of viscous dissipation

The effect of Eckert number Ec *i.e.*, viscous dissipation along with time τ on temperature profile and local Nusselt number is deliberated in Figs. 12 and 13. The negative values of Ec $(=-0.1)$ represent the cooling of the fluid, while positive values $(Ec = 0.1)$ represent the heating of the fluid and $Ec = 0$ indicates there is no viscous dissipation. The fluid's temperature enhances for both steady and unsteady cases and the energy transport rate diminishes when the viscous dissipation parameter (Ec) increases, due to the collision between the fluid particles. Particularly, heat transfer rate diminishes by approximately 56% when Ec increases from 0 to 0.1. Also, it is evident from Fig. 13 that, as time upsurges heat transfer rate also enhances for accelerating flow and opposite trend can be seen for decelerating flow.

5.6. Entropy and Bejan number

Figs. 14–18 elucidate the variations of local entropy generation (E_G) and Bejan number (Be) for different Brinkman number Br, temperature ratio parameter Ω_T, time τ and diffusion parameters

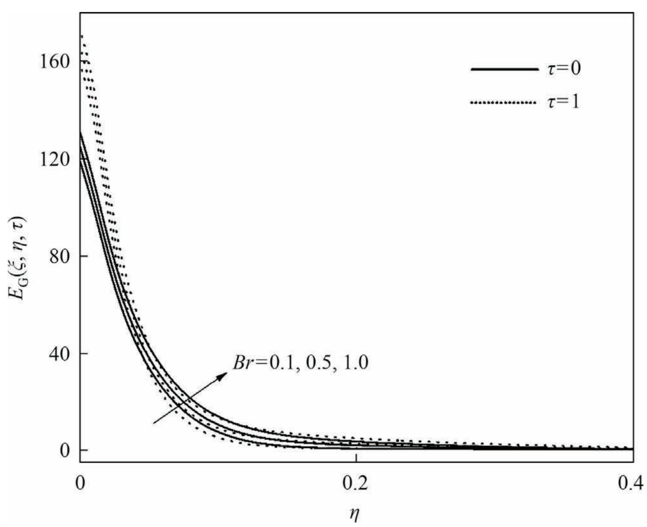

Fig. 14. Effect of Br on entropy generation for $\phi(\tau) = 1 + \alpha\tau^2$, $\alpha = 0.5$, when $\theta_w = 1.5$, $Ri = 10$, $\xi = 0.5$, $Re = 10$, $\beta_t = \beta_{c_1} = \beta_{c_1} = Nc_1 = Nc_2 = R_d = 0.1$, $M_1 = M_2 = M_3 = 0.5$, and $\Omega_T = \Omega_{c_1} = \Omega_{c_2} = 0.5$.

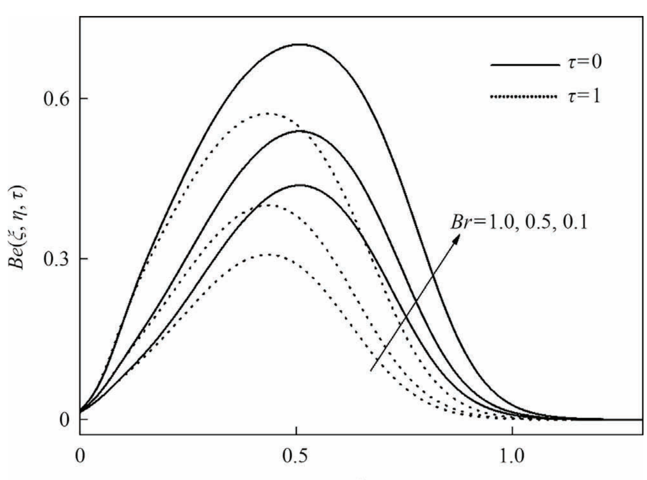

Fig. 15. Effect of Br on Bejan number $Be(\xi, \eta, \tau)$ for $\phi(\tau) = 1 + \alpha\tau^2$, $\alpha = 0.5$,when $\theta_w = 1.5$, $Ri = 10$, $\xi = 0.5$, $Re = 10$, $\beta_t = \beta_{c_1} = \beta_{c_1} = Nc_1 = Nc_2 = R_d = 0.1$, $M_1 = M_2 = M_3 = 0.5$, and $\Omega_T = \Omega_{c_1} = \Omega_{c_2} = 0.5$.

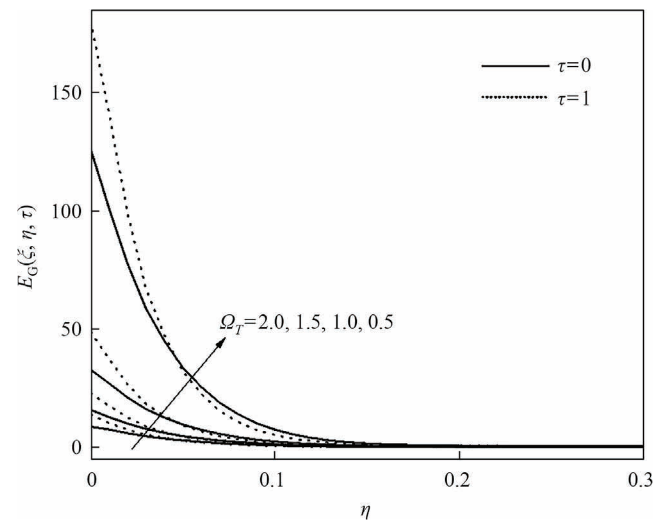

Fig. 16. Effect of Ω_T on entropy generation for $\phi(\tau) = 1 + \alpha\tau^2$, $\alpha = 0.5$, when $\theta_w = 1.5$, $Ri = 10$, $\xi = 0.5$, $Re = 10$, $\Omega_{c_1} = \Omega_{c_2} = 0.5$, $Br = 0.1$, $M_1 = M_2 = M_3 = 0.5$ and $\beta_t = \beta_{c_1} = \beta_{c_1} = Nc_1 = Nc_2 = R_d = 0.1$.

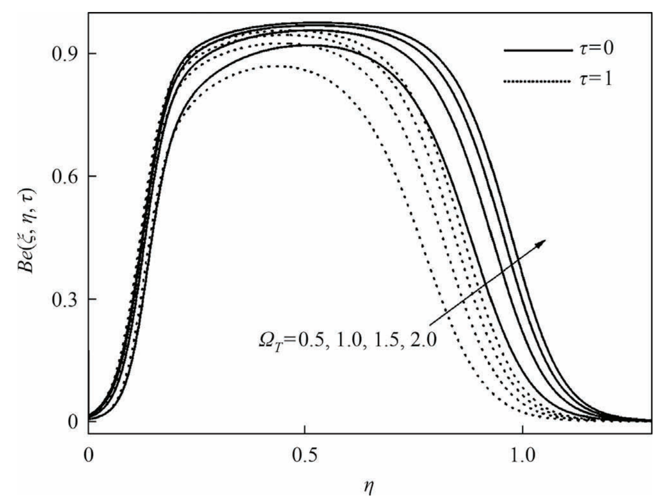

Fig. 17. Effect of Ω_T on Bejan number $Be(\xi, \eta, \tau)$ for $\phi(\tau) = 1 + \alpha\tau^2$, $\alpha = 0.5$, when $\theta_w = 1.5$, $Ri = 10$, $\xi = 0.5$, $Re = 10$, $Br = 0.1$, $\beta_t = \beta_{c_1} = \beta_{c_1} = Nc_1 = Nc_2 = R_d = 0.1$, $M_1 = M_2 = M_3 = 0.5$, and $\Omega_{c_1} = \Omega_{c_2} = 0.5$

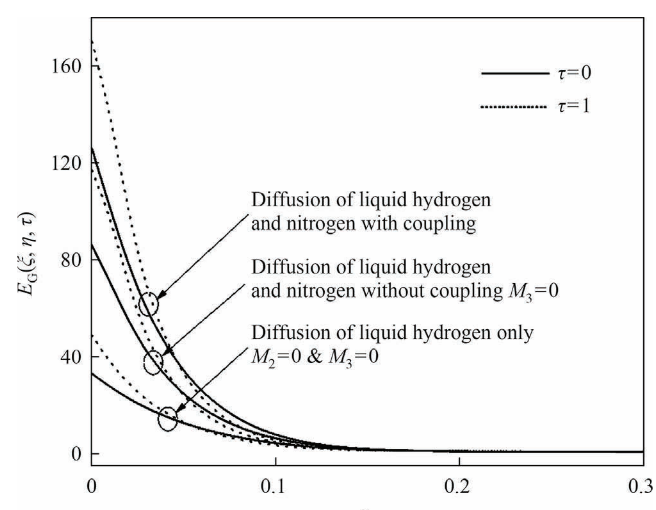

Fig. 18. Effects of M_1, M_2 and M_3 on entropy generation for $\phi(\tau) = 1 + \alpha\tau^2$, $\alpha = 0.5$, when $\theta_w = 1.5$, $Ri = 10$, $\xi = 0.5$, $Re = 10$, $Br = 0.1$, $\beta_t = \beta_{c_1} = \beta_{c_1} = Nc_1 = Nc_2 = R_d = 0.1$, and $\Omega_T = \Omega_{c_1} = \Omega_{c_2} = 0.5$.

M_1, M_2 and M_3. It is evident from the figures that EG and Bejan number possess opposite nature as they are inversely proportional. Figs. 14 and 15 demonstrate that the magnitude of E_G enhances and *Be* reduces for higher values of the *Br*. This is because, higher magnitude of the *Br* rises the frictional heating, causing extra energy to the fluid particles, which is the reason behind generating an enormous amount of entropy near the surface. The enhancing values of Ω_T declines the magnitude of E_G, while it surges the magnitude of *Be*. It is noted that the effect of Ω_T is better noticeable away from the surface.

Furthermore, the higher values of Ω_T reduces the heat transfer, fluid friction and diffusion irreversibility. Thus, the magnitude of E_G is reduced, and *Be* is enhanced.This is due to the fact that higher values of Ω_T signifies that the temperature of the fluid is more. Also, it is evident from the figures that, as time enhances, the magnitude of *Be* is reduced and E_G surged. Further, Fig. 18 deliberate the importance of time, diffusing components with and without coupling effects. The entropy generation is minimum for double diffusion (diffusion of liquid hydrogen only) than the triple diffusion (diffusion of liquid hydrogen and nitrogen) with and without coupling the diffusing components. Entropy generation is more when coupling of the diffusion components is considered. The coupling of diffusing components caused by concentration gradients has a significant impact on the entropy generation. Also, it is confirmed that the magnitude of E_G is more pronounced for $\tau = 1$ in all cases.

6. Conclusions

The following inferences are made upon studying the effects of various parameters over different profiles and gradients:

- The enhancing values of Ω_T declines the magnitude of E_G, while it surges the magnitude of *Be*.
- The entropy generation is minimum for double diffusion (diffusion of liquid hydrogen and heat only) than the triple diffusion (diffusion of liquid hydrogen, nitrogen and heat) with and without coupling the diffusing components.
- The mass transfer strength of liquid nitrogen is about 44% more than that of liquid hydrogen at $\tau = 1, \alpha = 0.5$, $A = 0.5$. *i.e.*, liquid nitrogen is a better coolant than liquid hydrogen.
- The enhancing values of R_d and θ_w augments the fluid temperature for both $\tau = 0$ and $\tau \neq 0$, concurrently declines the $Re_x^{-1/2} Nu$.
- When comparing the nonlinear thermal radiation withthe non-radiation case, the local Nusselt number is lowered by around 58% at $\tau = 1$, $R_d = 1$, $\theta_w = 1.5$, $\alpha = 0.5$.
- The energy transport strength is approximately 140% more for the permeable surface than the impermeable one, in case of suction at $\tau = 1$ when $\xi = 0.5$, $\alpha = 0.5$.
- The local energy transport strength and friction coefficient at the surface enhance approximately 50% and 87%, respectively, when *Ri* increments from –1 to 10 at $\tau = 1$, $\beta_t = 1$ and $\alpha = 0.5$.

Declaration of Competing Interest

The authors declare that they have no known competing financial interests or personal relationships that could have appeared to influence the work reported in this paper.

Acknowledgements

The second author is thankful for financial support to the Department of Science and Technology-Innovation in Science Pursuit for Inspired Research (DST-INSPIRE), New Delhi with the grant No. DST/INSPIRE Fellowship/[IF190225] dated 21-11-2020.

Nomenclature

A	*suction/injection attribute*
Be	Bejan number
Br	Brinkman number
C_f	local friction coefficient at the surface
C_j	species concentration
C_p	specific heat
D_{s_j}	Mass diffusivity
Ec	Eckert number
f	nondimensional stream function
$F=F_\eta$	nondimensional velocity
G	nondimensional temperature
g	acceleration due to gravity
H,S	nondimensional species concentration of liquid hydrogen and nitrogen
K	thermal conductivity
k^*	mean absorption coefficient
M_i	diffusion parameters
Nc_1, Nc_2	buoyancy ratio attributes for liquid hydrogen and nitrogen
Nu	local energy transfer rate
Pr	Prandtl number
q_r	radiative heat flux
R_d	dimensionless nonlinear thermal radiation parameter
R^*	gas constant
r_0	radius of the slender cylinder
Ri	Richardson number
Sc_j	Smidt number
Sh_j	local mass transfer rate
T	temperature of the fluid
T_w	wall temperature
T_∞	ambient fluid temperature
t	time
U_e	mainstream velocity
U_∞	mainstream velocity constant
u,v	components of velocity along x and r directions, respectively
x,r	axial and radial coordinates
α	unsteady parameter
β_1,β_2	coefficients of linear and quadratic thermal expansion
β_3,β_4	liquid hydrogen's linear and quadratic concentration expansion coefficients
β_5,β_6	liquid nitrogen's linear and quadratic concentration expansion coefficients
β_t	quadratic convectionparameter for temperature
β_{c_1}	quadratic convectionparameter for liquid hydrogen
β_{c_2}	quadratic convectionparameter for liquid nitrogen
θ_w	temperature ratio parameter
ξ, η	Transformed variables
ρ	density of the fluid
σ^*	Stefan–Boltzmann constant
τ	nondimensional time
$\phi(\tau)$	unsteady function of τ
ψ	stream function
Ω_{c_1}	ratio of liquid hydrogen concentration
Ω_{c_2}	ratio of liquid nitrogen concentration
Ω_T	ratio of temperature difference

Subscripts

w, ∞	constraints at the surface and away from the surface, respectively
ξ, η	partial derivatives with respect to ξ, η

References

[1] A. Noor, R. Nazar, K. Naganthran, I. Pop, Unsteady mixed convection flow at a three-dimensional stagnation point, *Int. J. Numer. Methods Heat Fluid Flow* 31 (1) (2021) 236–250.

[2] M. Kumari, G. Nath, Doubly diffusive unsteady mixed convection flow over a vertical plate embedded in a porous medium, *Int. J. Energy Res.* 13 (4) (1989) 419–430.

[3] M. Ghalambaz, S.A.M. Mehryan, A. Hajjar, A. Veismoradi, Unsteady natural convection flow of a suspension comprising Nano-Encapsulated Phase Change Materials (NEPCMs) in a porous medium, *Adv. Powder Technol.* 31 (3) (2020) 954–966.

[4] S. Roy, D. Anilkumar, Unsteady mixed convection from a moving vertical slender cylinder, *J. Heat Transf.* 128 (4) (2006) 368–373.

[5] Z.H. Khan, W.A. Khan, J.G. Tang, M.A. Sheremet, Entropy generation analysis of triple diffusive flow past a horizontal plate in porous medium, *Chem. Eng. Sci.* 228 (2020) 115980.

[6] M. Ghalambaz, F. Moattar, M.A. Sheremet, I. Pop, Triple-diffusive natural convection in a square porous cavity, *Transp. Porous Media* 111 (1) (2016) 59–79.

[7] W.A. Khan, J.R. Culham, Z.H. Khan, I. Pop, Triple diffusion along a horizontal plate in a porous medium with convective boundary condition, *Int. J. Therm. Sci.* 86 (2014) 60–67.

[8] P.M. Patil, M. Roy, S. Roy, E. Momoniat, Triple diffusive mixed convection along a vertically moving surface, *Int. J. Heat Mass Transf.* 117 (2018) 287–295.

[9] P.M. Patil, A. Shashikant, P.S. Hiremath, E. Momoniat, Influence of surface roughness on multidiffusive mixed convective nanofluid flow, *Phys. Scr.* 94 (5) (2019) 055201.

[10] P.M. Patil, M. Kulkarni, J.R. Tonannavar, A computational study of the triple-diffusive nonlinear convective nanoliquid flow over a wedge under convective boundary constraints, *Int. Commun. Heat Mass Transf.* 128 (2021) 105561.

[11] M. Ghalambaz, F. Moattar, A. Karbassi, M.A. Sheremet, I. Pop, Triple-diffusive mixed convection in a porous open cavity, *Transp. Porous Media* 116 (2) (2017) 473–491.

[12] A.Z. Al-Garni, A.Z. Sahin, B.S. Yilbas, S.A. Ahmed, Cooling of aerospace plane using liquid hydrogen and methane, *J. Aircr.* 32 (3) (1995) 539–546.

[13] P. Smakulski, S. Pietrowicz, Dynamics of liquid nitrogen cooling process of solid surface at wetting contact coefficient, *IOP Conf. Ser.: Mater. Sci. Eng.* 101 (2015) 012037.

[14] Universal Industrial Gases Inc. USA. Nitrogen (N2) properties, uses, application: Nitrogen gas and liquid nitrogen, 2018. https://www.uigi.com/nitogen.html.

[15] T.S. Chen, A. Mucoglu, Bouyancy effects on forced convection along a vertical cylinder, *J. Heat Transf.* 97 (2) (1975) 198–203.

[16] S.L. Lee, T.S. Chen, B.F. Armaly, Mixed convection along vertical cylinders and needles with uniform surface heat flux, *J. Heat Transf.* 109 (3) (1987) 711–716.

[17] J.J. Heckel, T.S. Chen, B.F. Armaly, Mixed convection along slender vertical cylinders with variable surface temperature, *Int. J. Heat Mass Transf.* 32 (8) (1989) 1431–1442.

[18] T.Y. Wang, C. Kleinstreuer, General analysis of steady laminar mixed convection heat transfer on vertical slender cylinders, *J. Heat Transf.* 111 (2) (1989) 393–398.

[19] P.J. Singh, S. Roy, I. Pop, Unsteady mixed convection from a rotating vertical slender cylinder in an axial flow, *Int. J. Heat Mass Transf.* 51 (5–6) (2008) 1423–1430.

[20] M. Kumari, G. Nath, Mixed convection boundary layer flow over a thin vertical cylinder with localized injection/suction and cooling/heating, *Int. J. Heat Mass Transf.* 47 (5) (2004) 969–976.

[21] O. Aydin, A. Kaya, MHD-mixed convection from a vertical slender cylinder, *Commun. Nonlinear Sci. Numer. Simul.* 16 (4) (2011) 1863–1873.

[22] H.S. Takhar, A.J. Chamkha, G. Nath, Combined heat and mass transfer along a vertical moving cylinder with a free stream, *Heat Mass Transf.* 36 (3) (2000) 237–246.

[23] P.M. Patil, S. Roy, A.J. Chamkha, P.S. Kulkarni, Unsteady mixed convection flow from a moving vertical slender cylinder in the presence of viscous dissipation, *Int. J. Microscale Nanoscale Therm. Fluid Transp. Phenom.* 2 (4) (2011) 281–305.

[24] P.M. Patil, S. Roy, I. Pop, Chemical reaction effects on unsteady mixed convection boundary layer flow past a permeable slender vertical cylinder due to a nonlinearly stretching velocity, *Chem. Eng. Commun.* 200 (3) (2013) 398–417.

[25] K.U. Rehman, M.Y. Malik, O.D. Makinde, Parabolic curve fitting study subject to Joule heating in MHD thermally stratified mixed convection stagnation point flow of Eyring-Powell fluid induced by an inclined cylindrical surface, *J. King Saud Univ. Sci.* 30 (4) (2018) 440–449.

[26] A. Bejan, A study of entropy generation in fundamental convective heat transfer, *J. Heat Transf.* 101 (4) (1979) 718–725.

[27] S.E. Ahmed, Z.A.S. Raizah, A.M. Aly, Entropy generation due to mixed convection over vertical permeable cylinders using nanofluids, *J. King Saud Univ. Sci.* 31 (3) (2019) 352–361.

[28] N.S. Khan, Q. Shah, A. Bhaumik, P. Kumam, P. Thounthong, I. Amiri, Entropy generation in bioconvection nanofluid flow between two stretchable rotating disks, *Sci. Rep.* 10 (2020) 4448.

[29] M.I. Khan, M.U. Hafeez, T. Hayat, M.I. Khan, A. Alsaedi, Magneto rotating flow of hybrid nanofluid with entropy generation, *Comput. Methods Programs Biomed.* 183 (2020).

[30] F. Haq, M. Saleem, M.I. Khan, Y. Elmasry, R. Chinram, Entropy generation minimization in bio-convective flow of nanofluid with activation energy and gyrotactic micro-organisms, *AIP Adv.* 11 (5) (2021) 105093.

[31] A. Sahoo, R. Nandkeolyar, Entropy generation and dissipative heat transfer analysis of mixed convective hydromagnetic flow of a Casson nanofluid with thermal radiation and Hall Current, *Sci. Rep.* 11 (2021) 3926.

[32] S.Z. Abbas, M.I. Khan, S. Kadry, W.A. Khan, M.I. Rehman, M. Waqas, Fully developed entropy optimized second order velocity slip MHD nanofluid flow with activation energy, *Comput. Methods Programs Biomed.* 190 (2020) 105362.

[33] M.I. Khan, S. Kadry, Y.M. Chu, M. Waqas, Modeling and numerical analysis of nanoliquid (titanium oxide, graphene oxide) flow viscous fluid with second order velocity slip and entropy generation, *Chin. J. Chem. Eng.* 31 (2021) 17–25.

[34] S. Shaw, A.S. Dogonchi, M.K. Nayak, O.D. Makinde, Impact of entropy generation and nonlinear thermal radiation on Darcy-Forchheimer flow of MnFe2O4-casson/water nanofluid due to a rotating disk: Application to brain dynamics, *Arab. J. Sci. Eng.* 45 (7) (2020) 5471–5490.

[35] M.I. Afridi, M. Qasim, O.D. Makinde, Entropy generation due to heat and mass transfer in a flow of dissipative elastic fluid through a porous medium, *J. Heat Transf.* 141 (2) (2019) 022002.

[36] M.I. Afridi, M. Qasim, N.A. Khan, O.D. Makinde, Minimization of entropy generation in MHD mixed convection flow with energy dissipation and joule heating: Utilization of sparrow-quack-boernerlocal non-similarity method, Defect Diffusion, *Forum* 387 (2018) 63–77.

[37] M. Hassan, S. Ali, W. Aich, F. Khlissa, B. Ayadi, L. Kolsi, Transport pattern of Non-Newtonian mass and thermal energy under two diverse flow conditions by using modified models for thermodynamics properties, *Case Stud. Therm. Eng.* 29 (2022) 101714.

[38] L. Kolsi, S. Dero, L.A. Lund, U.F. Alqsair, M. Omri, S.U. Khan, Thermal stability and performances of hybrid nanoparticles for convective heat transfer phenomenon with multiple solutions, *Case Stud. Therm. Eng.* 28 (2021) 101684.

[39] K. Vajravelu, K.S. Sastri, Fully developed laminar free convection flow between two parallel vertical walls—I, *Int. J. Heat Mass Transf.* 20 (6) (1977) 655–660.

[40] R. Bhargava, R.S. Agarwal, Fully developed free convection flow in a circular pipe, *Ind. J. Pure Appl. Math.* 10 (1979) 357–365.

[41] P.M. Patil, I. Pop, S. Roy, Unsteady heat and mass transfer over a vertical stretching sheet in a parallel free stream with variable wall temperature and concentration, *Numer. Methods Partial. Differ. Equ.* 28 (3) (2012) 926–941.

[42] I.C. Mandal, S. Mukhopadhyay, Nonlinear convection in micropolar fluid flow past an exponentially stretching sheet in an exponentially moving stream with thermal radiation, *Mech. Adv. Mater. Struct.* 26 (24) (2019) 2040–2046.

[43] A.S. Eegunjobi, O.D. Makinde, Inherent irreversibility in a reactive and radiating magnetic nanoliquid film along a slippery inclined heated surface with convective cooling, *Heat Transf.* 49 (3) (2020) 1533–1553.

[44] D.D. Gray, A. Giorgini, The validity of the boussinesq approximation for liquids and gases, *Int. J. Heat Mass Transf.* 19 (5) (1976) 545–551.

[45] H. Schlichting, K. Gersten, Boundary-layer Theory, Springer, New York, 2000.

[46] J.R. Radbill, G.A. McCue, Quasilinearization and Nonlinear Problem in Fluid and Orbital Mechanics, Elsevier, Amsterdam, 1970.

[47] R.E. Bellman, R.E. Kalaba, Quasilinearization and Nonlinear Boundary Value Problems, Elsevier, New York, 1965.

[48] K. Inouye, A. Tate, Finite-difference version of quasi-linearization applied to boundary-layer equations, *AIAA J.* 12 (4) (1974) 558–560.

[49] P.M. Patil, D.N. Latha, S. Roy, E. Momoniat, Non-similar solutions of mixed convection flow from an exponentially stretching surface, *Ain Shams Eng. J.* 8 (4) (2017) 697–705.

[50] P.M. Patil, M. Kulkarni, P.S. Hiremath, Effects of surface roughness on mixed convective nanofluid flow past an exponentially stretching permeable surface, *Chin. J. Phys.* 64 (2020) 203–218.

[51] R.S. Varga, Matrix Iterative Analysis, Springer, Berlin, 2000.

[52] C.A. Scribd, Mass diffusivity data, https://www.scribd.com/doc/58782633/Mass Diffusivity-Data.